Exploring the Binding Conformations of Bulkier Dipeptide Amide Inhibitors in Constitutive Nitric Oxide Synthases†

Huiying Li,‡ Mack L. Flinspach,‡ Jotaro Igarashi,‡ Joumana Jamal,‡ Weiping Yang,‡ José Antonio Gómez-Vidal,§ Elizabeth A. Litzinger,§ Hui Huang,§ Erik P. Erdal,§ Richard B. Silverman, and Thomas L. Poulos*,‡

Departments of Molecular Biology and Biochemistry, Chemistry, and Physiology and Biophysics and the Center in Chemical and Structural Biology, University of California, Irvine, California 92697-3900, and Department of Chemistry, Department of Biochemistry, Molecular Biology, and Cell Biology and the Center for Drug Discovery and Chemical Biology, Northwestern University, Evanston, Illinois 60208-3113

Received July 13, 2005; Revised Manuscript Received September 19, 2005

ABSTRACT: A series of L-nitroarginine-based dipeptide inhibitors are highly selective for neuronal nitric oxide synthase (nNOS) over the endothelial isoform (eNOS). Crystal structures of these dipeptides bound to both isoforms revealed two different conformations, curled in nNOS and extended in eNOS, corresponding to higher and lower binding affinity to the two isoforms, respectively. In previous studies we found that the primary reason for selectivity is that Asp597 in nNOS, which is Asn368 in eNOS, provides greater electrostatic stabilization in the inhibitor complex. While this is the case for smaller dipeptide inhibitors, electrostatic stabilization may no longer be the sole determinant for isoform selectivity with bulkier dipeptide inhibitors. Another residue farther away from the active site, Met336 in nNOS (Val106 in eNOS), is in contact with bulkier dipeptide inhibitors. Double mutants were made to exchange the D597/M336 pair in nNOS with N368/V106 in eNOS. Here we report crystal structures and inhibition constants for bulkier dipeptide inhibitors bound to nNOS and eNOS that illustrate the important role played by residues near the entry to the active site in isoform selective inhibition.

Nitric oxide synthases (NOS[1]) catalyze the oxidation of an L-arginine guanidinium nitrogen atom to nitric oxide (NO), a potent biological signaling molecule that mediates a diverse range of physiological processes within the nervous, immune, and cardiovascular systems (*1*, *2*). Three mammalian NOS isoforms, neuronal (nNOS), inducible NOS (iNOS), and endothelial (eNOS), share a common modular architecture consisting of a C-terminal reductase domain and an N-terminal catalytic oxygenase domain connected by a calmodulin-binding linker (*3*, *4*). The various NOS isoforms are functional as homodimers with the dimer forming between the heme domains. The reductase domain houses the FAD and FMN cofactors that shuttle electrons from NADPH to the heme domain where oxygen activation and substrate hydroxylation occur.

Unregulated production of NO contributes to a large number of pathological conditions. A locally high concentration of NO generated by hyperactive iNOS and nNOS has been identified as the cause of various human diseases. Cerebral ischemic damage in stroke is related to NO release by nNOS (*5*, *6*). Chronic neurodegenerative diseases such as Parkinson's (*7*) and chronic inflammatory diseases such as arthritis (*8*) and colitis (*9*) are directly linked to NO overproduction by iNOS. The pancreatic β-cell death associated with diabetes was also caused by the iNOS-produced NO (*10*). On the other hand, endothelial dysfunction owing to impaired NO production by eNOS leads to disease states such as hypertension (*11*) and atherosclerosis (*12*).

Owing to these many pathological conditions in addition to the basic physiological functions associated with NOS, indiscriminate inhibition of NOS would be detrimental. Therefore, isoform-selective inhibition is an important pharmaceutical goal (*13*−*16*). A majority of the known inhibitors of NOS are targeted to the heme domain where they block L-Arg binding. The crystal structures of the dimeric heme domain for all three mammalian NOS isoforms are known (*17*−*20*) which have opened the way for structure-based inhibitor design. This has proven to be a challenging problem since the active site architectures of the three isoforms are so similar. Nevertheless, we have been able to uncover the primary structural feature that controls isoform selectivity in a group of dipeptide inhibitors (Figure 1) (*21*) that exhibit up to a 2000-fold selectivity for nNOS over eNOS (*22*−*25*). As shown in Figure 2, **I** and **III** bind very differently to nNOS and eNOS. In nNOS these inhibitors adopt a curled conformation which places the inhibitor α-amino group between two active site carboxylates, Glu592 and Asp597, with a direct H-bond to Glu592. In eNOS, the inhibitors adopt the fully extended conformation and in the

† This research was supported by NIH Grants GM57353 (T.L.P) and GM49725 (R.B.S.).

* Corresponding author. E-mail: poulos@uci.edu. Tel: 949-824-7020. Fax: 949-824-3280.

‡ University of California.

§ Northwestern University.

[1] Abbreviations: NOS, nitric oxide synthase; nNOS, neuronal NOS; eNOS, endothelial NOS; iNOS, inducible NOS; H_4B, (6*R*)-5,6,7,8-tetrahydrobiopterin; 2′,5′-ADP, 2′,5′-adenosine diphosphate; δ-Ala, 5-aminolevulinic acid; GSH, glutathione reduced; IPTG, isopropyl β-D-1-thiogalactopyranoside; MES, 2-morpholinoethanesulfonic acid; NTA, nitrilotriacetic acid; TCEP, tris-(2-carboxyethyl)-phosphine hydrochloride.

10.1021/bi0513610 CCC: $30.25 © 2005 American Chemical Society
Published on Web 10/29/2005

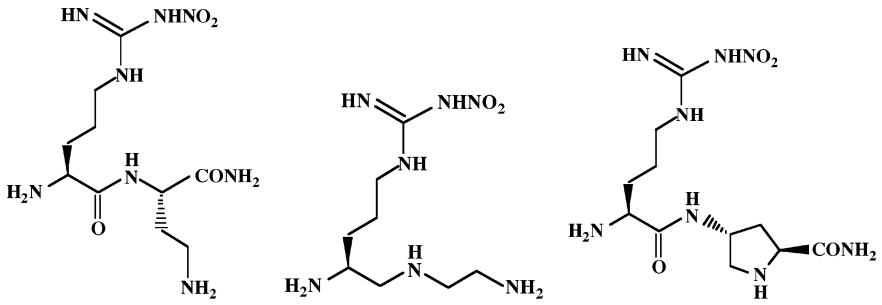

I **II** **III**

FIGURE 1: Chemical structures and nomenclature of the dipeptide amide inhibitors: **I**, L-N^{ω}-nitroarginine-2,4-L-diaminobutyramide; **II**, **(**4*S*)-*N*-(4-amino-5-[aminoethyl]aminopentyl)-*N*′-nitroguanidine; **III**, L-N^{ω}-nitroarginine-(4*R*)-amino-L-proline amide.

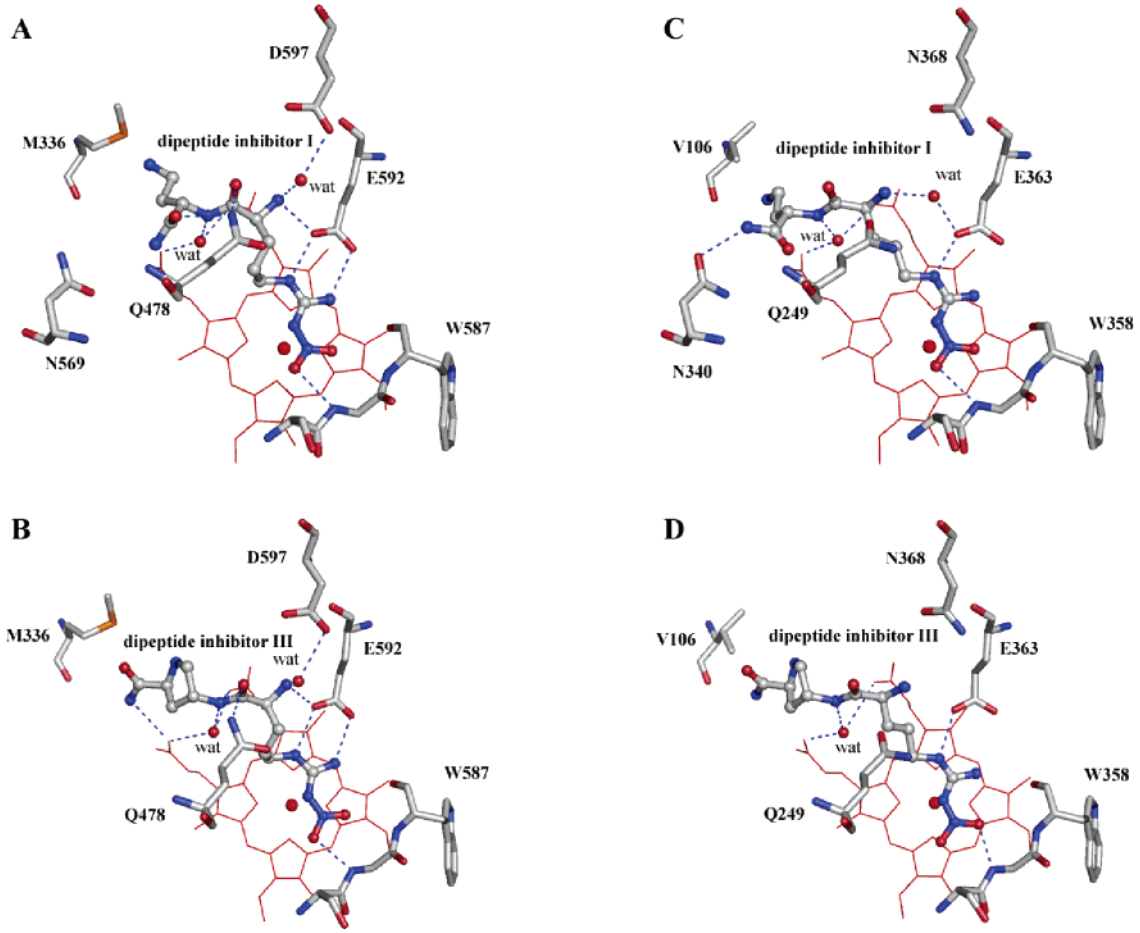

FIGURE 2: The active site structures of dipeptide **I** and **III**, respectively, bound to the wild-type nNOS (A and B) and eNOS (C and D). H-bonds are depicted with dashed lines. The atomic color schemes are carbon in gray, oxygen red, nitrogen blue, and sulfur orange. Figures were made with PYMOL (www.pymol.org).

case of **I** a water molecule is situated between the inhibitor α-amino group and Glu363, the homologue to Glu592 in nNOS. We hypothesized that the curled vs extended conformation is due to a single amino acid difference, Asp597 in nNOS which is Asn368 in eNOS. Since nNOS has two carboxylates in the active site, there is additional electrostatic stabilization of the inhibitor α-amino group positive charge in nNOS compared to eNOS. To test this hypothesis we replaced Asp597 with Asn in nNOS and Asn368 with Asp in eNOS. **I** binds to the eNOS mutant in the curled conformation exactly as in wild-type nNOS, and K_i decreases about 10-fold (Table 1). In the nNOS mutant **I** binds in the extended conformation exactly as in wild-type eNOS with an increase in K_i of about 220-fold (*21*). Although this single amino difference accounts for the difference in inhibitor conformation, the K_i for the eNOS mutant for **I** is 9.5 μM

Table 1: Inhibitory Potency (K_i in μM) and Binding Modes of Dipeptide Amides

	dipeptide **I**		dipeptide **III**	
	K_i (μM)	binding mode	K_i (μM)	binding mode
wild-type eNOS	107.0	extended	110.0	extended
wild-type nNOS	0.30	curled	0.10	curled
eNOS N368D	9.5	mixed	5.1	curled
eNOS N368D/V106M	1.7	n/a	1.1	curled
nNOS D597N	67.0	extended	20.0	mixed
nNOS D597N/M336V	63.3	extended	42.0	curled

while for wild-type nNOS $K_i = 0.30$ μM. Therefore, the single amino acid difference accounts for most but not all the difference in K_i.

A closer examination of the structures (Figure 2) reveals additional differences closer toward the entry to the active site near the H_4B binding site where there is Val106 in eNOS but Met336 in nNOS. We reasoned that the larger Met side chain may impose greater steric restraints that sequester the inhibitor more tightly into the active site. Indeed, the inhibitor nitro group is significantly closer to the backside wall of the active site in nNOS where Gly586 and Trp587 locate (Gly357 and Trp358 in eNOS). With many inhibitor−NOS complex structures in hand we have not so far observed any ligand binding induced conformational changes in the protein backbone although some residues lining the active site channel undergo small changes owing to the enzyme−inhibitor interactions. To test the role of the Met/Val difference, we have generated nNOS and eNOS double mutants where the Asp/Met pair in nNOS are converted to Asn/Val as well as the reciprocal mutants with eNOS. Here we report the crystal structures of the single and double mutants of nNOS and eNOS complexed with **I** and **III** as well as K_i values for **I** and **III** for both wild-type and mutant nNOS and eNOS.

EXPERIMENTAL PROCEDURES

Synthesis of Dipeptide Amides and Determination of K_i Values. The chemical syntheses of **I** and **III** have been described previously (*22*, *25*). Nitric oxide formation was monitored by the hemoglobin capture assay (*26*). The K_i values were obtained following the method of Dixon (*27*). Initial reaction velocities were measured using at least four different inhibitor concentrations at four different substrate concentrations: 10, 6, 4, and 2 μM L-arginine. The measurements for each substrate concentration were plotted as a line, with the deviation from the mean of the measurements being less than ±5%. These lines were then plotted on the same graph, and points of intersection within ±7% of each other were averaged to give the mean $-K_i$.

Protein Preparation and Purification. Both bovine eNOS and rat nNOS were expressed in the *Escherichia coli* strain BL21(DE3) using a pCWori vector as described (*20*, *21*). The eNOS N368D/V106M double mutant was generated with the overlap extension procedure (28) using the plasmid of N368D construct as a template in PCR to amplify the fragment between *Nde*I and *Kpn*I sites within the eNOS coding region. The PCR fragment was then agarose gel purified and ligated back to the wild-type eNOS plasmid which had been double digested with *Nde*I and *Kpn*I. A similar technique was used to generate nNOS D597N/M336V mutant from D597N construct using *Nde*I and *Aat*II sites for cloning.

Protein expression was carried out with BL21(DE3) *E. coli* strain as the expression host using TB culture. Although NOS can be expressed alone in *E. coli*, an improved expression yield can be achieved by coexpression with human calmodulin. *E. coli* cells were transformed by plasmid pACYC/CaM (a generous gift from Dr. Paul Ortiz de Montellano's lab) to make competent cells, which were then transformed a second time with pCWori/NOS plasmid (either eNOS or nNOS) in the presence of both ampicillin and chloramphenicol for coexpression of CaM and NOS. Colonies grown in the LB agar plate with both antibiotics were used to inoculate a small volume of LB culture and grown at 37 °C overnight. Each 1 L TB culture in a 2.8 L Fernbach flask was then inoculated by 3 mL of overnight LB starter. The cultures were allowed to grow at 37 °C with 220 rpm agitation until the OD at 600 nm reached 1.5. Cultures were then induced by 0.5 mM IPTG, 0.4 mM δ-Ala, and 3 μM riboflavin. Postinduction incubation at 25 °C with 100 rpm agitation for another 40 h was found to give the best protein yield.

The full-length NOS protein is usually purified using Ni NTA or 2′,5′-ADP sepharose column, and if necessary the combination of the two columns as described previously (*20*, *21*). To avoid competitive binding of imidazole with some weaker inhibitors, certain batches of NOS proteins were purified off the Ni NTA column using histidine to replace imidazole as the eluent. When copurification of CaM is not desired, 5 mM EGTA can be added to the buffer after the NTA column step to remove Ca^{2+} ion therefore stripping off CaM. The heme domain proteins used for crystallographic studies were generated by restricted trypsin digest and then further purified through a Superdex 200 column, also described before (*21*).

Crystallization of Inhibitor−NOS Complex. The heme domains of NOS samples used for crystallization were usually purified in the absence of L-Arg (or imidazole in some cases) to avoid competition with the inhibitor binding. Protein samples at 7−10 mg/mL were incubated with 8 mM of a dipeptide inhibitor before setting up the sitting drops on glass cover slips using Q plate (Hampton Reaserch). The reservoir solution for eNOS contains 15−20% (v/v) PEG3350, 100 mM Na cacodylate, pH 6.0−7.0, 100−200 mM Mg acetate, 5 mM TCEP, whereas the reservoir for nNOS includes 20−24% (v/v) PEG3350, 100 mM MES, pH 5.6−6.0, 100−200 mM ammonium acetate, 35 μM SDS, 5.0 mM GSH. Both eNOS and nNOS crystals reach their full size in 2 days at 5−7 °C and retain their best diffraction power within 10 days.

Diffraction Data Collection, Processing, and Structure Refinement. X-ray diffraction data collections were carried out at either Advance Light Source (ALS, Berkeley, CA) or Stanford Synchrotron Radiation Laboratory (SSRL, Palo Alto, CA) at 100 K using a CCD detector. Data frames were processed with HKL2000 (29). The binding of inhibitors was detected by calculating the $F_o - F_c$ difference Fourier density maps using CNS (*30*) with F_c and phases provided by the previously refined nNOS or eNOS heme domain model excluding the active site ligand and water molecules. The structure refinements were also done using CNS with manual model manipulations using the graphic program O (*31*) between each round of minimization and *B* factor refinement. Water molecules were automatically picked with CNS but visually inspected in O. The refined models were checked using online RCSB validation tools. The coordinates along with the structure factors of these structures have been deposited with the RCSB protein data bank. The crystal diffraction data collection and model refinement statistics are summarized in Table 2.

RESULTS AND DISCUSSION

Binding Affinities of Dipeptides to eNOS and nNOS Double Mutants. K_i values for **I** and **III** bound to the wild-type and

Table 2: Data Collection and Refinement Statistics

data set:[a]	**III** with nNOS D597N	**III** with nNOS D597N/M336V	**I** with nNOS D597N/M336V	**III** with eNOS N368D	**III** with eNOS N368D/V106M
PDB code	1ZZQ	1ZZR	1ZZU	1ZZS	1ZZT
cell dimens (Å) (space group: $P2_12_12_1$)					
a	51.59	52.43	52.36	57.87	56.45
b	109.81	111.95	111.13	107.06	105.74
c	164.67	164.83	165.16	156.79	155.60
data resolution (Å)	1.90	2.05	1.90	1.85	2.14
total observations	366 514	227 072	277 503	281 507	195 244
unique reflections	74 155	60 961	75 577	88 824	54 826
Rsym[b]	0.086	0.064	0.030	0.067	0.055
	(0.561)[c]	(0.532)	(0.131)	(0.455)	(0.359)
$\langle I/\sigma \rangle$	8.9	8.9	23.4	11.7	23.8
	(3.1)[c]	(2.0)	(7.7)	(2.0)	(2.3)
completeness (%)	99.7	99.1	99.2	97.9	99.2
	(100.0)[c]	(93.7)	(95.1)	(99.4)	(99.5)
reflections used in refinement	740 81	60 889	75 522	82 165	51 861
R factor[d]	0.220	0.227	0.202	0.175	0.189
R-free[e]	0.244	0.260	0.228	0.211	0.233
no. of protein atoms	6683	6657	6657	6441	6441
no. of heterogen atoms	245	193	209	197	181
no. of water molecules	516	407	683	652	372
RMS deviation					
bond length (Å)	0.009	0.010	0.008	0.010	0.010
bond angle (deg)	1.4	1.5	1.4	1.5	1.6

[a] **I**: L-N^{ω}-nitroarginine-2,4-L-diaminobutyramide. **III**: L-N^{ω}-nitroarginine-(4*R*)-amino-L-proline amide. [b] Rsym $= \sum|I - \langle I \rangle|/\sum I$, where I is the observed intensity of a reflection and $\langle I \rangle$ the averaged intensity of multiple observations of the reflection and its symmetry mates. [c] The values in parentheses were obtained in the outermost resolution shell. [d] R factor $= \sum||F_o| - |F_c||/\sum|F_o|$. F_o and F_c are the observed and calculated structure factors, respectively. [e] *R*-free was calculated with the 5% of reflections set aside randomly throughout the refinement. For each isoform, the same set of reflections were used for all data sets.

mutant eNOS and nNOS are presented in Table 1. For both inhibitors, the order of increasing affinity for the inhibitors to eNOS is double mutant > single mutant > wild-type. The K_i value for **I** is 1.7 μM for the eNOS double mutant compared to 9.5 μM for the single mutant while for **III** the K_i values are 1.1 μM and 5.1 μM, respectively. Therefore, the second mutation of eNOS, V106M, increases affinity for both **I** and **III** over the single mutants by a factor of 5.6 and 4.6, respectively. The newly established contacts with the bulkier Met side chain to the inhibitors apparently contribute favorably to the binding affinity. With nNOS, the second mutation has a less dramatic effect. In the case of **I** there is no difference between the single and double mutants while for **III** the second mutation decreases binding affinity by 2-fold.

*Binding of **III** to nNOS and eNOS Single Mutants.* Figures 3A and C show the binding of **III** in the nNOS D597N and the eNOS N368D single mutants, respectively. The binding of **III** to the eNOS N368D mutant is clearly in the curled conformation, the α-amino group of **III** being directly H-bonded to the Glu363 side chain, exactly as in the wild-type nNOS. However, in the D597N nNOS mutant the electron density is less well defined and supports binding in both the curled and extended conformations. The inhibitor structure beyond the peptide bond is disordered, making modeling of the two alternate conformations for the (4*R*)-amino-L-proline-amide moiety ambiguous. A perturbation of the Arg481 side chain is observed (Figure 3A) which indicates that the peptide carbonyl group in one of the conformers of **III** must be in the vicinity of Arg481. The altered side chain conformation of Arg481 triggers an alternate rotamer of Ser477, which, in turn, provides an additional H-bond to mannitol, an ingredient in the cryoprotectant for crystals, making the bound sugar clearly visible in electron density. Mannitol is located in a groove close to the active site entrance in nNOS (Figure 4). Although mannitol has been used for all nNOS structures we have solved, we do not normally observe well-ordered electron density for mannitol except for those structures where the dipeptide inhibitor binding causes alternate side chain conformation of both Arg481 and Ser477 (*32*). The H-bond to mannitol provided by the Ser477 side chain in its alternate rotamer is likely the key to ordering of mannitol such that it now can be seen in the electron density maps. Thus, the strong electron density for mannitol observed in the **III**−nNOS single mutant complex is an indicator of the direct interactions between **III** and Arg481. Note that the extended conformation of **III** seen in the nNOS D597N mutant (Figure 3A) is not the same as that in the wild-type eNOS (Figure 2D). The L-proline amide tail of **III** is most likely in the vicinity of Asn569, whereas in the wild-type eNOS−**III** complex the L-proline amide tail stretches outward toward the entry to the active site and takes full advantage of the wider binding pocket in eNOS created by a smaller Val106 side chain which is Met336 in nNOS. As a result, the guanidinium group of L-nitroarginine also has shifted outward, which weakens one of the two H-bonds from the guanidinium nitrogens to the Glu363 carboxylate oxygens. In contrast, a bulkier Met336 side chain in nNOS at the equivalent position of Val106 of eNOS may not allow the tail of dipeptide **III** to extend so far out of the active site, thus discouraging the inhibitor from adopting an extended conformation in nNOS even after removal of the negative charge at position 597 by Asp to Asn mutation. We therefore changed Met336 to Val in nNOS in order to create enough space to accommodate dipeptide **III** in its extended conformation.

*Binding of **I** and **III** to nNOS and eNOS Double Mutants.* Figures 3B and D show **III** binding to the nNOS D597N/M336V and eNOS N368D/V106M double mutants, respectively, while Figure 3E shows **I** complexed to the nNOS double mutant. Similar to the nNOS single mutant (*20*, *21*),

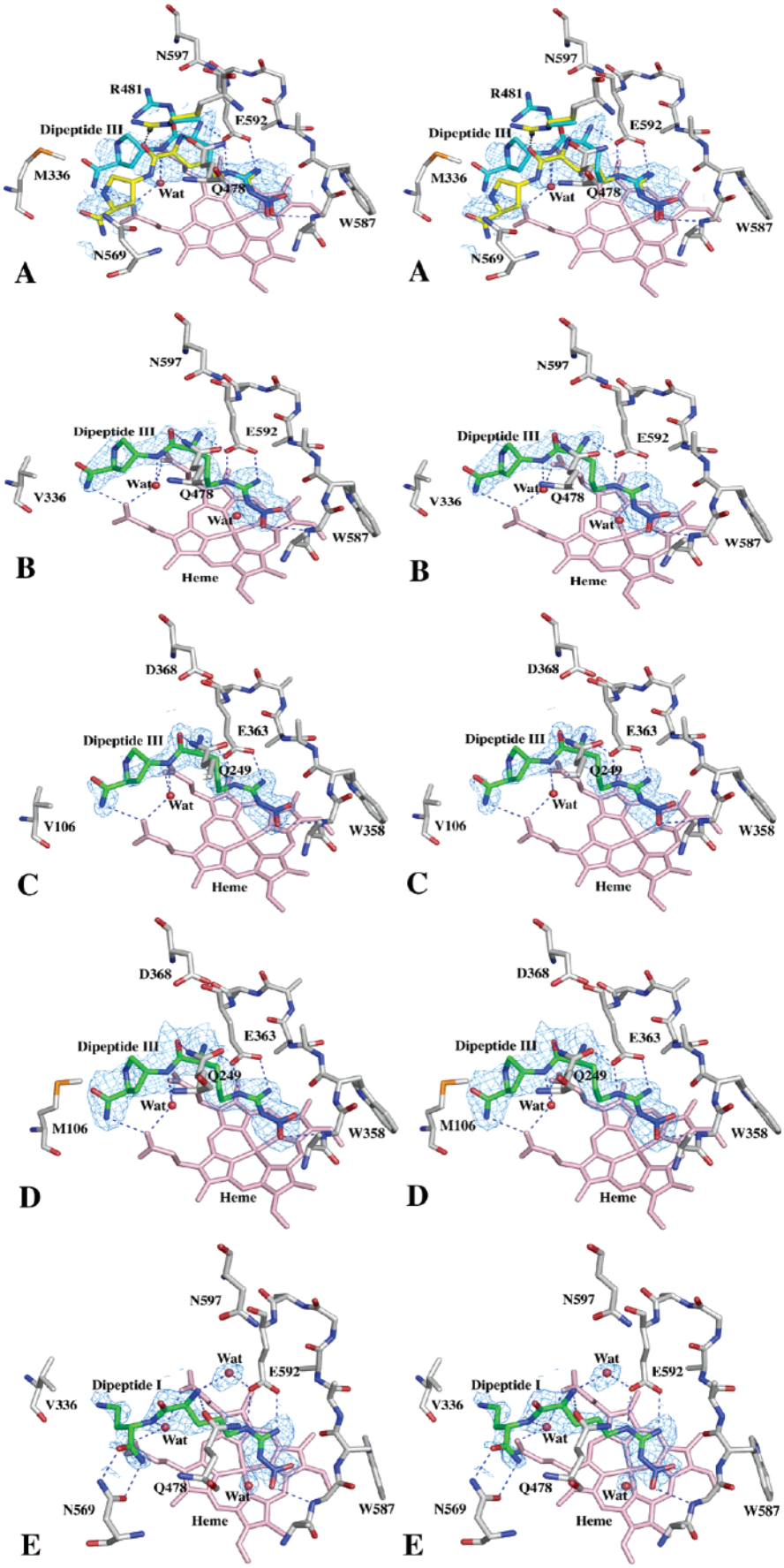

FIGURE 3: Stereoviews of the dipeptide binding in five new complex structures with $F_o - F_c$ omit electron density maps contoured at 3σ around the inhibitor: (A) **III** with nNOS D597N; (B) **III** with nNOS D597N/M336V; (C) **III** with eNOS N368D; (D) **III** with eNOS N368D/V106M; (E) **I** with nNOS D597N/M336V. For clarity only the labeled residues are shown with side chains.

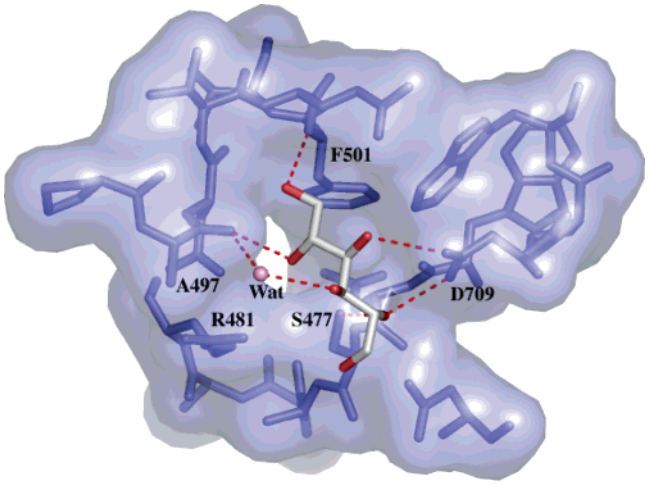

FIGURE 4: Mannitol binding to a protein groove shown as the van der Waals surface. Four of the six mannitol single OH groups are H-bonded to protein groups. Ser477 adopts an alternate rotamer which enables the Ser447 side chain OH to H-bond with mannitol and is a key feature in making mannitol clearly visible in electron density maps in the **III**−nNOS D597N and **I**−nNOS D597N/M336V structures.

I is found in an extended conformation in the nNOS double mutant. We also note that, when **I** binds in the extended conformation in both nNOS single and double mutants, the close interactions between **I** and Arg481 also lead to alternate side chain conformations of Arg481 and Ser477 making mannitol binding observable. Also as expected, **III** binds unambiguously in the curled conformation to the eNOS double mutant, which is similar to how **III** binds to the eNOS N368D single mutant (Figure 3C). To our surprise, however, **III** binds to the nNOS double mutant in the curled conformation (Figure 3B). In fact the electron density for the double mutant is much cleaner than in the single mutant (compare Figures 3A and 3B). There is no sign of mannitol binding, which implies that there is not an alternate conformer of **III**. It thus appears that the **III**−nNOS double mutant complex violates the "rule" that an Asn at position 597 (368 in eNOS) leads to an extended conformation (see Table 1). Moreover, changing Met336 to Val should have further promoted the extended conformation but just the opposite occurred.

We believe that the reason for the unexpected binding mode of **III** to the nNOS double mutant is due to interactions between the protein and amide tail of the inhibitor. Thus far we have focused solely on the strong H-bonding interactions between the inhibitor α-amino group and active site carboxylates. However, the tail of the inhibitor also forms H-bonding interactions that favor either the curled or the extended conformation. For **III** there is a rich set of interactions between the tail amide group and surrounding protein that would be weakened if the inhibitor adopted the extended conformation (compare Figures 2B and 2D). One of the main interactions that would be lost is the H-bond between the **III** amide and the heme propionate. This is not the case with **I**. In **I** the amide is positioned quite differently (Figure 1) and does not have the same favorable interactions with heme propionate in the curled conformation. In the extended conformation **I** can establish other new interactions such as the H-bonds between its amide group and Asn569 in nNOS (Asn340 in eNOS, Figures 2C and 3E). When an Asn is at position 597 in nNOS (368 in eNOS), these new interactions can tip the energetic balance making the extended conformation more favorable than the curled one. Therefore, **I** adopts the extended conformation in the nNOS double mutant exactly as in wild-type eNOS.

This still leaves open the question of why **III** adopts the extended conformation in wild-type eNOS when it should, based on the above discussion, adopt the curled conformation just as with the nNOS double mutant. The most probable explanation is due to another amino acid difference between eNOS and nNOS. As shown in Figure 5, His373 in eNOS (Ser602 in nNOS) is part of an H-bonding network involving a glycerol molecule that bridges between His373 and **III**. These interactions would be lost in the curled conformation. The smaller Ser602 in nNOS cannot form the same set of H-bonds found in eNOS and, hence, there is no energetic incentive for **III** to adopt the extended conformation in the nNOS double mutant even though a glycerol molecule is present next to H_4B in the structure. It thus appears that the curled vs extended conformation of **III** is in part a consequence of the high glycerol concentrations required for cryoprotection. When glycerol is removed from consideration, as would be the case in buffers used for K_i measurements, we would expect **III** to adopt predominantly the curled conformation, which is required to maintain favorable interactions between the protein and tail amide group.

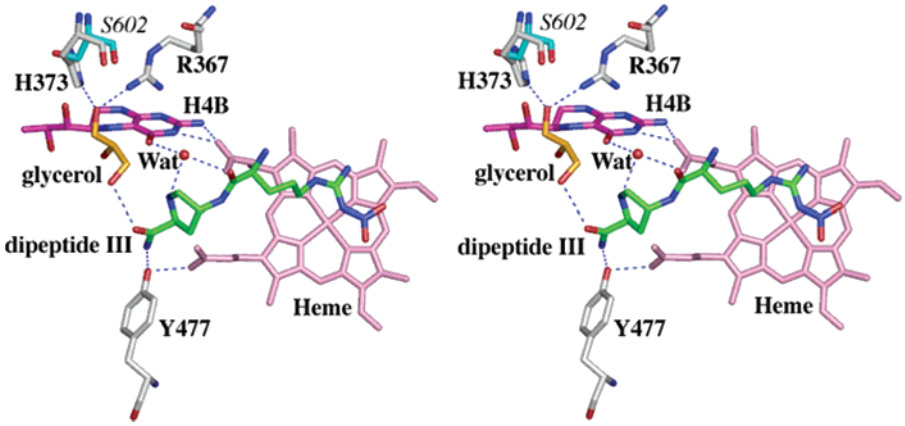

FIGURE 5: Stereoview of the H-bonding network involving His373, glycerol, and dipeptide **III** in the wild-type eNOS that stabilizes **III** in its extended conformation. In the **III**−nNOS D597N/M336V mutant complex structure the lack of such an extensive H-bonding network due to a smaller Ser602 at the position of His373 of eNOS might be the reason for **III** to still adopt the curled conformation.

CONCLUSIONS

Our current studies together with those previously published (*32*) were designed to test the hypothesis that two critical differences in the NOS active site contribute isoform-selective binding by a series of dipeptide inhibitors (Figure 1). The most important is the Asp/Asn difference between nNOS and eNOS where the Asp597 in nNOS provides greater electrostatic stabilization of the inhibitor α-amino group than the Asn368 in eNOS. If, however, this were the only feature causing the difference in inhibitory potency, then the K_i values for the N368D eNOS mutant should match those for wild-type nNOS. This is not the case. The tails of these inhibitors extend out of the active site where interactions occur between other side chains that differ between eNOS and nNOS. Based on our previous work, we hypothesized that the smaller Val106 side chain in eNOS near the active site entry allows inhibitors to adopt the extended conformation while the larger Met336 in nNOS provides closer steric interactions, which encourages the curled conformation. **I** nicely follows this pattern. As shown in Table 1, K_i for eNOS goes from 107 μM for wild-type, to 9.5 μM for the N368D mutant, and to 1.7 μM for the N368D/V106M mutant. If we take wild-type nNOS as the target, $K_i = 0.3$ μM, the eNOS double mutant accounts for all but a factor of 5−6 of the difference in binding of **I** to wild-type eNOS and nNOS. **III** follows a similar pattern with eNOS since the K_i drops in going from wild-type to the single and double mutants (Table 1). **I** and **III** binding to nNOS, however, is more complex. While the K_i increases in going from wild-type to the single and double mutants, the difference between the single and double mutants is only 2-fold for **III** and nothing for **I**. Nearly all the difference in K_i for both **I** and **III** in nNOS is due to changing Asp597 to Asn with little contribution from changing Met336 to Val. Thus our initial hypothesis that both electrostatic interactions involving the active site Asp and the steric restraint provided by Met336 in nNOS holds up for eNOS but is more tenuous with nNOS. This discrepancy is probably due to the richer sets of interactions that occur between the inhibitors and protein when the inhibitor is in the extended conformation. The farther from the conserved active site core, the greater the sequence diversity and, hence, the greater the differences in interactions the inhibitor tail can experience between NOS isoforms. For example, the His373 in eNOS vs Ser602 in nNOS provides quite different H-bonding, steric, and electrostatic sets of interactions with the tail of the inhibitor. This also will result in differences in solvent structure near the active site entrance. Given this scenario, it might be possible to exploit the greater sequence diversity around the active site entry in order to design novel inhibitors with greater isoform selectivity.

ACKNOWLEDGMENT

We would like to acknowledge the assistance we received from the beamline staff at SSRL and ALS during synchrotron data collection.

REFERENCES

1. Moncada, S., Palmer, R. M., and Higgs, E. A. (1991) Nitric oxide: physiology, pathophysiology, and pharmacology, *Pharmacol. Rev. 43*, 109−142.
2. Kerwin, J. F., Jr., Lancaster, J. R., Jr., and Feldman, P. L. (1995) Nitric oxide: a new paradigm for second messengers, *J. Med. Chem. 38*, 4343−4362.
3. Griffith, O. W., and Stuehr, D. J. (1995) Nitric oxide synthases: properties and catalytic mechanism, *Annu. Rev. Physiol. 57*, 707−736.
4. Masters, B. S., McMillan, K., Sheta, E. A., Nishimura, J. S., Roman, L. J., and Martasek, P. (1996) Neuronal nitric oxide synthase, a modular enzyme formed by convergent evolution: structure studies of a cysteine thiolate-liganded heme protein that hydroxylates L-arginine to produce NO. as a cellular signal, *FASEB J. 10*, 552−558.
5. Lipton, P. (1999) Ischemic cell death in brain neurons, *Physiol. Rev. 79*, 1431−1568.
6. Sims, N. R., and Anderson, M. F. (2002) Mitochondrial contributions to tissue damage in stroke, *Neurochem. Int. 40*, 511−526.
7. Liberatore, G. T., Jackson-Lewis, V., Vukosavic, S., Mandir, A. S., Vila, M., McAuliffe, W. G., Dawson, V. L., Dawson, T. M., and Przedborski, S. (1999) Inducible nitric oxide synthase stimulates dopaminergic neurodegeneration in the MPTP model of Parkinson disease, *Nat. Med. 5*, 1403−1409.
8. Bingham, C. O., 3rd (2002) The pathogenesis of rheumatoid arthritis: pivotal cytokines involved in bone degradation and inflammation, *J. Rheumatol., Suppl. 65*, 3−9.
9. Kankuri, E., Vaali, K., Knowles, R. G., Lahde, M., Korpela, R., Vapaatalo, H., and Moilanen, E. (2001) Suppression of acute experimental colitis by a highly selective inducible nitric-oxide synthase inhibitor, N-[3-(aminomethyl)benzyl]acetamidine, *J Pharmacol. Exp. Ther. 298*, 1128−1132.
10. Mandrup-Poulsen, T. (1996) The role of interleukin-1 in the pathogenesis of IDDM, *Diabetologia 39*, 1005−1029.
11. Taddei, S., Virdis, A., Ghiadoni, L., Sudano, I., and Salvetti, A. (2001) Endothelial dysfunction in hypertension, *J. Cardiovasc. Pharmacol. 38*, Suppl. 2, S11−14.
12. Rekka, E. A., and Chrysselis, N. C. (2002) Nitric oxide in atherosclerosis, *Mini-Rev. Med. Chem. 2*, 433−445.
13. Hobbs, A. J., Higgs, A., and Moncada, S. (1999) Inhibition of nitric oxide synthase as a potential therapeutic target, *Annu. Rev. Pharmacol. Toxicol. 39*, 191−220.
14. Southan, G. J., and Szabo, C. (1996) Selective pharmacological inhibition of distinct nitric oxide synthase isoforms, *Biochem. Pharmacol. 51*, 383−394.
15. Babu, B. R., and Griffith, O. W. (1998) Design of isoform-selective inhibitors of nitric oxide synthase, *Curr. Opin. Chem. Biol. 2*, 491−500.
16. Alderton, W. K., Cooper, C. E., and Knowles, R. G. (2001) Nitric oxide synthases: structure, function and inhibition, *Biochem. J. 357*, 593−615.
17. Crane, B. R., Arvai, A. S., Ghosh, D. K., Wu, C., Getzoff, E. D., Stuehr, D. J., and Tainer, J. A. (1998) Structure of nitric oxide synthase oxygenase dimer with pterin and substrate, *Science 279*, 2121−2126.
18. Raman, C. S., Li, H., Martasek, P., Kral, V., Masters, B. S., and Poulos, T. L. (1998) Crystal structure of constitutive endothelial nitric oxide synthase: a paradigm for pterin function involving a novel metal center, *Cell 95*, 939−950.
19. Fischmann, T. O., Hruza, A., Niu, X. D., Fossetta, J. D., Lunn, C. A., Dolphin, E., Prongay, A. J., Reichert, P., Lundell, D. J., Narula, S. K., and Weber, P. C. (1999) Structural characterization of nitric oxide synthase isoforms reveals striking active-site conservation, *Nat. Struct. Biol. 6*, 233−242.
20. Li, H., Shimizu, H., Flinspach, M., Jamal, J., Yang, W., Xian, M., Cai, T., Wen, E. Z., Jia, Q., Wang, P. G., and Poulos, T. L. (2002) The novel binding mode of N-alkyl-N′-hydroxyguanidine to neuronal nitric oxide synthase provides mechanistic insights into NO biosynthesis, *Biochemistry 41*, 13868−13875.
21. Flinspach, M. L., Li, H., Jamal, J., Yang, W., Huang, H., Hah, J. M., Gomez-Vidal, J. A., Litzinger, E. A., Silverman, R. B., and Poulos, T. L. (2004) Structural basis for dipeptide amide isoform-selective inhibition of neuronal nitric oxide synthase, *Nat. Struct. Mol. Biol. 11*, 54−59.
22. Huang, H., Martasek, P., Roman, L. J., Masters, B. S., and Silverman, R. B. (1999) N(omega)-Nitroarginine-containing dipeptide amides. Potent and highly selective inhibitors of neuronal nitric oxide synthase, *J. Med. Chem. 42*, 3147−3153.

23. Huang, H., Martasek, P., Roman, L. J., and Silverman, R. B. (2000) Synthesis and evaluation of peptidomimetics as selective inhibitors and active site probes of nitric oxide synthases, *J. Med. Chem. 43*, 2938−2945.
24. Hah, J. M., Roman, L. J., Martasek, P., and Silverman, R. B. (2001) Reduced amide bond peptidomimetics. (4S)-N−(4-amino-5-[aminoakyl]aminopentyl)-N′-nitroguanidines, potent and highly selective inhibitors of neuronal nitric oxide synthase, *J. Med. Chem. 44*, 2667−2670.
25. Gomez-Vidal, J. A., Martasek, P., Roman, L. J., and Silverman, R. B. (2004) Potent and selective conformationally restricted neuronal nitric oxide synthase inhibitors, *J. Med. Chem. 47*, 703−710.
26. Hevel, J. M., and Marletta, M. A. (1994) Nitric-oxide synthase assays, *Methods Enzymol. 233*, 250−258.
27. Dixon, M. (1953) The Determination of Enzyme Inhibitor Constants, *Biochem. J. 55*, 170.
28. Ho, S. N., Hunt, H. D., Horton, R. M., Pullen, J. K., and Pease, L. R. (1989) Site-directed mutagenesis by overlap extension using the polymerase chain reaction, *Gene 77*, 51−59.
29. Otwinowski, Z., and Minor, W. (1997) Processing of X-ray diffraction data collected in oscillation mode, *Methods Enzymol. 276*, 307−326.
30. Brunger, A. T., Adams, P. D., Clore, G. M., DeLano, W. L., Gros, P., Grosse-Kunstleve, R. W., Jiang, J.-S., Kuszewski, J., Nilges, M., Pannu, N. S., Read, R. J., Rice, L. M., Simonson, T., and Warren, G. L. (1998) Crystallography & NMR System: A new software suite for macromolecular structure determination, *Acta Crystallogr. D54*, 905−921.
31. Jones, T. A., Zou, J.-Y., Cowan, S. W., and Kjeldgaarrd, M. (1991) Improved methods for building models in electron density and the location of errors in these models, *Acta Crystallogr. A47*, 110−119.
32. Flinspach, M., Li, H., Jamal, J., Yang, W., Huang, H., Silverman, R. B., and Poulos, T. L. (2004) Structures of the neuronal and endothelial nitric oxide synthase heme domain with D-nitroarginine-containing dipeptide inhibitors bound, *Biochemistry 43*, 5181−5187.

BI0513610